

Supporting Information for

Mass Transfer-Limited Biodegradation at Low Concentrations— Evidence from Reactive Transport Modeling of Isotope Profiles in a Bench-Scale Aquifer

Fengchao Sun^{†,‡}, Adrian Mellage[§], Mehdi Gharasoo^{†,£}, Aileen Melsbach^{†,‡}, Xin Cao[Ⓔ], Ralf Zimmermann[Ⓔ], Christian Griebler[Ⓟ], Martin Thullner[¶], Olaf A. Cirpka[§], and Martin Elsner^{,†,‡}*

[†]Institute of Groundwater Ecology, Helmholtz Zentrum München, Ingolstädter Landstrasse 1, 85764 Neuherberg, Germany

[‡] Chair of Analytical Chemistry and Water Chemistry, Technical University of Munich, Marchioninistrasse 17, 81377 Munich, Germany

[§] Center for Applied Geoscience, University of Tübingen, Schnarrenbergstrasse 94–96, 72076 Tübingen, Germany

[£] Department of Earth and Environmental Sciences, Ecohydrology, University of Waterloo, 200 University Avenue West, Waterloo, Canada

[Ⓔ] Joint Mass Spectrometry Centre, Comprehensive Molecular Analytics (CMA) Cooperation Group Helmholtz Zentrum, Gmunderstrasse 37, 81379 Munich, Germany

[Ⓟ] Department of Functional and Evolutionary Ecology, University of Vienna, Althanstrasse 14, 1090 Vienna, Austria

[¶] Department of Environmental Microbiology, UFZ—Helmholtz Centre for Environmental Research, Permoserstrasse 15, 30418 Leipzig, Germany

SUMMARY

17 pages, 3 figures and 2 table

CONTENTS

Chemicals	3
Sample Preparation and Solid-phase Extraction (SPE)	3
BAM and 2,6-DCBA Concentration Measurements on LC-MS/MS	4
Table S1. Parameters of target analytes on MS	4
Carbon and Nitrogen Isotope Measurements on GC-IRMS	4
Medium Preparation and Bacteria Cultivation	6
Set-up of the Two-dimensional Flow-through Sediment-Tank Experiment	6
Additional Equations for the Mass-Transfer Limitation Scenario	7
Governing Equations for the Scenario without Mass-Transfer Limitation	7
Parameter Uncertainties and Sensitivities	8
Table S2. Flow and transport parameters and reaction rate coefficients, for the reactive transport model	10
Figure S1. Parameter sensitivities plotted at each measurement location.	12
Derivation of the Apparent Enrichment Factor (Equation 18)	13
Additional Supporting Figures	16
Figure S2. Simulated transient development of $\Delta\delta^{13}\text{C}$, $c_{\text{bulk}}^{\text{BAM}}$, and TCC	16
Figure S3. Concentration difference between $c_{\text{bulk}}^{\text{BAM}}$ and $c_{\text{int}}^{\text{BAM}}$	16
References	17

Chemicals

The following chemicals were used: 2,6-dichlorobenzamide (Sigma Aldrich, Germany), 2,6-dichlorobenzamide-3,4,5-d₃, 98.4%-d₃ (Alfa Chemistry, Ronkonkoma, NY).

The following chemicals were used for the medium preparation: disodium phosphate (6 g/L), monopotassium phosphate ($\geq 99\%$), ammonium chloride ($\geq 99\%$), magnesium sulfate heptahydrate ($\geq 98\%$), calcium chloride dihydrate ($\geq 99\%$), boric acid ($\geq 99.5\%$), manganese sulfate monohydrate ($\geq 99\%$), copper sulfate pentahydrate ($\geq 98\%$), zinc chloride ($\geq 98\%$), cobalt chloride hexahydrate ($\geq 98\%$), sodium molybdate monohydrate ($\geq 99\%$), glucose, and ferric chloride ($\geq 98\%$). All the chemicals were from Sigma Aldrich, Germany.

Sample Preparation and Solid-phase Extraction (SPE)

Samples for carbon and nitrogen isotope analysis were filtered through 0.2 μM PES filter (Nalgene Thermo Scientific, Germany) and frozen at $-20\text{ }^{\circ}\text{C}$ immediately after each sampling event until enough sample volume (2 L) was collected. Samples for concentration measurements were filtered through 0.22 μM syringe filters (Merck KGaA, Germany), adjusted to pH 1.7 with HCl and spiked with internal standard 2,6-dichlorobenzamide-3,4,5-d₃ before solid phase extraction (SPE). The SPE method was adapted from Torrentó et al.¹ and Jensen et al.². For the SPE of isotope samples, 0.2 g of hydrophobic polymer-based sorbent Bakerbond SDB-1 (J.T. Baker, USA) was self-packed into empty 6 mL PP SPE cartridges with PE frit (20 μm pore size; Sigma Aldrich, Germany). The cartridges were conditioned with 3 mL ethyl acetate, followed by 2×3 mL methanol and 2×3 mL Milli-Q water. 200 – 2000 mL samples were loaded to the SPE columns at a rate of 3 mL/min. After sample loading, the cartridges were washed twice with 3 mL of Milli-Q water and dried for 2 hours. BAM was eluted with 3 mL ethyl acetate, dried under a gentle stream of nitrogen at room temperature, and re-dissolved in 100–1000 μl ethyl acetate for CSIA. For the SPE method of concentration samples, 50 mg sorbent was packed in the 1 mL empty PP SPE cartridge with PE frit (20 μm pore size; Sigma Aldrich, Germany). The cartridges were conditioned with 1 mL ethyl acetate, followed by 2×1 mL methanol and 2×1 mL Milli-Q water. 1 mL samples were slowly loaded to the SPE columns. After sample loading, the cartridges were washed twice with 1 mL Milli-Q water and dried for 1 hour. Compounds were eluted with 1 mL acetonitrile, dried under a gentle stream of nitrogen at room temperature, and re-dissolved in 100-1000 μl 10% acetonitrile water solution for LC-MS/MS measurements.

BAM and 2,6-DCBA Concentration Measurements on LC-MS/MS

The method of the concentration measurement of BAM and 2,6-DCBA on LC-MS/MS was adapted from Jensen et al.² Briefly, liquid chromatography (LC) was performed on an Agilent 1100 HPLC system including a column compartment, an autosampler, a binary pump system, and a degasser (Agilent Technologies Inc, USA). Mass spectrometry (MS) was operated on a QTrap 4000 system using electrospray ionization (ESI) (Sciex, USA). Separation was carried out on a Kinetex® C18 column (2.6 μm , 10 nm, 100 \times 2.1 mm i.d., Phenomenex, USA) at 40 °C. Mobile phase A was 5 mM of ammonium acetate with pH of 2.4 (adjusted by formic acid). Mobile phase B was acetonitrile. A gradient flow of 300 $\mu\text{L}/\text{min}$ was used as follows: 0–5 min, 90% A; 5–9 min, 90%–10% A; 9–10 min, 10%–90% A; 10–15 min, 90% A. The injection volume was 10 μL . Each sample was analyzed twice in multiple reaction monitoring (MRM) mode with a temperature of 450 °C, a nebulizer gas at 50 psi, a heater gas at 40 psi, a curtain gas at 20 psi, and a collision gas at 11 psi. 2,6-Dichlorobenzamide and 2,6-dichlorobenzamide-3,4,5- d_3 (internal standard) were analyzed in positive mode with a capillary voltage at 4.5 kV. 2,6-Dichlorobenzoic acid was analyzed in negative mode with a capillary voltage at -4.5 kV. For each sample, two transitions were selected. The first transition was used for quantification and the second transition was used for qualification (shown in Table S1).

Table S1. Parameters of target analytes on MS

Compound	Precursor ion (m/z)	Product ion (m/z)	Declustering potential (V)	Entrance potential (V)	Collision energy (V)	Cell exit potential (V)
2,6-Dichlorobenzamide	190	173	75	10	29	7
	190	145.3	75	10	40	7
2,6-dichlorobenzamide-3,4,5- d_3	193.1	176.1	70	10	27	7
	193.1	148.0	70	10	42	7
2,6-dichlorobenzoic acid	189	144.9	-26	-3	-13	-8
	189	35.2	-26	-3	-33	-3

Carbon and Nitrogen Isotope Measurements on GC-IRMS

This method was described by Sun et al³. Briefly, a TRACE GC Ultra gas chromatograph (Thermo Fisher Scientific, Italy) and a Finnigan MAT 253 isotope ratio mass spectrometer (IRMS) were coupled through a Finnigan GC Combustion III interface (Thermo Fisher Scientific, Germany). A DB-5 analytical column (30 m, 0.25 mm i.d., 0.5 μ m film, Agilent Technologies, Germany) was used to separate BAM in the gas chromatograph. Helium (grade 5.0) was the carrier gas. For the isotope measurement of the high BAM concentration samples, we used a Thermo injector in the split/split-less injection mode; for the isotope measurement of the low BAM concentration samples, we applied a programmable injector controlled by an Optic 3 system with liquid N₂-cryofocusing (ATAS GL, distributed by Axel Semrau, Germany) in on-column injection mode, in which a Rxi retention gap (fused silica, 3 m \times 0.53 mm inner diameter) (RESTEK, Germany) was connected to a custom made on-column liner.

In the split/split-less injection mode, the GC method started at 80 °C. At a ramp rate of 15 °C/min, temperature increased to 280 °C and was held for 7 min. The flow rate was kept constant at 1.4 mL/min. In the on-column injection mode, the GC oven started at 35 °C and was held for 30 s. At a ramp rate of 5 °C/min, temperature increased to 80 °C. Then at a ramp rate of 15 °C/min, temperature increased from 80 °C to 280 °C. In the Optic 3, the method started at an initial temperature of 40 °C and was held for 300 s. Then temperature increased to 250 °C at a ramp rate of 2 °C/s. The initial flow rate was 0.3 mL/min and was held for 120 s. Then it was increased to 1.4 mL/min within 2 min. Thus, before the GC temperature program started a stable flow rate of 1.4 mL/min was established.

We used Vienna PeeDee Belemnite (V-PDB) and Air-N₂ to determine the carbon isotope values $\delta^{13}\text{C}$ [‰] and nitrogen isotope values $\delta^{15}\text{N}$ [‰] of the samples. We calculated the carbon and nitrogen isotope values $\delta^{13}\text{C}$ and $\delta^{15}\text{N}$ of the samples in relation to a lab reference gas (CO₂ and N₂, respectively). In the beginning and the end of each run, the reference gas was measured against V-PDB and air by using international reference materials (provided by IAEA), e.g., the CO₂ gases RM 8562, RM8563 for CO₂, and RM 8564 and NSVEC (N₂) for N₂.

Medium Preparation and Bacteria Cultivation

The medium for the growth of *Aminobacter* sp. Strain MSH1 in the biotic tank experiment was adapted from Schultz-Jensen et al.⁴ Briefly, medium solution was prepared with Na₂HPO₄ (6 g/L), KH₂PO₄ (3 g/L), NH₄Cl (1 g/L), MgSO₄ × 7H₂O (0.2 g/L), CaCl₂ × 2H₂O (0.01 g/L) and autoclaved at 120 °C. After autoclaving, 10 mL from the trace element stock solution was filtered through 0.22 μm syringe filters (Merck KGaA, Germany) and added to 1 L medium solution. The trace elements stock solution was H₃BO₃ (39 mg/L), MnSO₄ × H₂O (84.5 mg/L), CuSO₄ × 5H₂O (125 mg/L), ZnCl₂ (69 mg/L), CoCl₂ × 6H₂O (119.5 mg/L), and Na₂MoO₄ × H₂O (121 mg/L).

Aminobacter sp. Strain MSH1 was from the Department of Geochemistry, the Geological Survey of Denmark and Greenland (GEUS), Denmark. The strain on the sterile plates was transferred to the medium solution with a sterile needle. Precultures were made in 1 L shaker flask containing 200 mL medium solution. 2 mL of autoclaved glucose were added to 200 mL medium solution as carbon source. To ensure that the culture maintain its BAM-degrading ability, BAM was added to the medium (10 mg/L). The preculture was incubated in an orbital shaker at 130 rpm at 20 °C until an optical density (OD) of 1 was reached. The preculture with OD = 1 was centrifuged in four 50 mL centrifuge tubes at 4000 rpm for 5 min. Cell pellets were resuspended and washed in 10 mL medium solution (without glucose or BAM) for three times to remove the remaining glucose or BAM in the preculture. Finally, the suspended bacterial cell pellets were resuspended in 2 L medium solution (without glucose or BAM); the experimental culture with OD value of 0.1 was ready for the inoculation to the tank.

Set-up of the Two-dimensional Flow-through Sediment Tank Experiment

The quasi-two-dimensional tank was made up of two glass plates, separated by a Teflon spacer, and all fitted into two aluminum rims at either side of the chamber which were screwed together. The tank respectively was fitted with sixteen, equally spaced (at 1.0 cm distance each), ports at the inlet and outlet to accurately inject different constituents at specified depths and to sample with a high depth resolution at the outlet. The inner dimensions of the domain were 95 cm × 18 cm × 1 cm (L × H × W), so that the tank represents a quasi-two-dimensional system. The tank was wet packed with sterilized sand (0.8–1.2 mm grain diameter). Stainless steel capillaries and tygon pump-tubes are used to connect to inflow and outflow peristaltic pumps (Ismatec, Germany). The pumping rate was maintained at 45 ± 2 μL/min per port. The

seepage velocity was 1.25 m/d. The tank was sterilized with 12 g/L NaOH solution and rinsed with autoclaved Milli-Q water before the experiment.

Additional Equations for the Mass-Transfer limitation Scenario

We assume that k_{tr} [1/s], the mass transfer rate coefficient, primarily describes the transfer through the cell membrane and neglect the transfer resistance from the bulk solution to the cell. The mass transfer through the cell membrane between the bulk phase and the cytoplasm has different effects on the bulk-phase concentration than on the intracellular concentrations because of the disproportionate bulk solution vs. single cell volumes. Therefore, eq 1, in the main manuscript, and the following equations, which describe the degradation rates in the bulk solution, contain the ratio of the biomass concentration over the mass density of bacterial cells. While the concentration in the cell interior may be expressed in moles of substrate per volume of pore space, this would not be the concentration experienced by the enzymes. Thus, comparisons between studies using pure enzymes and those involving bacterial cells may not be valid.

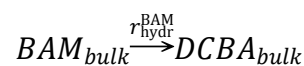
The fitted value of the coefficient, k_{tr} can be used to estimate the effective diffusion coefficient D_{eff} [m² s⁻¹], and the apparent permeability of the cell membrane P_{app} [m s⁻¹],⁵⁻⁷

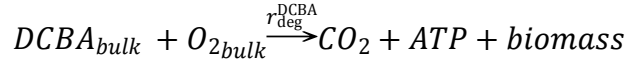
$$k_{tr} = \frac{P_{app} \times A_{cell}}{V_{cell}} = \frac{D_{eff} \times K_{lipw} \times A_{cell}}{\sigma \times V_{cell}} \quad (S1)$$

where K_{lipw} [L_{water} L_{membrane}⁻¹] (value of 11) is the lipid-water distribution coefficient of BAM,⁸ A_{cell} and V_{cell} are the surface area and volume of a single cell, 6 μm² and 0.9 μm³, respectively,⁹ ¹⁰ and we can assume that the diffusive distance, σ [nm], from the substrates in the bulk solution to the location of the enzyme is the thickness of two lipid bilayer of the gram-negative bacterial strain *Aminobacter* sp. MSH1, $\sigma = 10$ nm.^{11, 12}

Governing Equations for the Scenario without Mass-Transfer Limitation

In the simulation scenario without mass transfer limitation, the mass transfer process through the cell membrane was neglected, thus only the substrate concentrations in the bulk solution were simulated. The BAM degradation pathway can be simplified as,





in which BAM was irreversibly hydrolyzed to the main intermediate 2,6-DCBA via an amidase enzyme, then 2,6-DCBA is either degraded to CO₂ and ATP via aerobic respiration or utilized for the synthesis of biomass (C₅H₇O₂N).

The reactive transport of substrates in the bulk solution was coupled to microbial dynamics and was described by the following equations in two dimensions:

$$\frac{\partial c_{bulk}^{l,h,BAM}}{\partial t} = -\mathbf{v} \cdot \nabla c_{bulk}^{l,h,BAM} + \nabla \cdot (\mathbf{D}_{BAM} \cdot \nabla c_{bulk}^{l,h,BAM}) - {}^{l,h}r_{hydr}^{BAM} \quad (S2)$$

$$\frac{\partial c_{bulk}^{O_2}}{\partial t} = -\mathbf{v} \cdot \nabla c_{bulk}^{O_2} + \nabla \cdot (\mathbf{D}_{O_2} \cdot \nabla c_{bulk}^{O_2}) - r_{deg}^{O_2} \quad (S3)$$

$$\frac{\partial c_{bulk}^{DCBA}}{\partial t} = -\mathbf{v} \cdot \nabla c_{bulk}^{DCBA} + \nabla \cdot (\mathbf{D}_{DCBA} \cdot \nabla c_{bulk}^{DCBA}) + {}^l r_{hydr}^{BAM} + {}^h r_{hydr}^{BAM} - r_{deg}^{DCBA} \quad (S4)$$

$$\frac{\partial X^{im}}{\partial t} = r_{growth}^{im} - r_{daughter} - r_{decay}^{im} \quad (S5)$$

$$\frac{\partial X^{mob}}{\partial t} = -\mathbf{v} \cdot \nabla X^{mob} + \nabla \cdot (\mathbf{D} \cdot \nabla X^{mob}) + r_{daughter} \quad (S6)$$

$${}^l r_{hydr}^{BAM} = r_{max}^{hydro} \cdot \frac{{}^l c_{bulk}^{BAM}}{c_{bulk}^{BAM_{total}} + K_m^{BAM}} \quad (S7)$$

$${}^h r_{hydr}^{BAM} = \alpha \cdot r_{max}^{hydro} \cdot \frac{{}^h c_{int}^{BAM}}{c_{bulk}^{BAM_{total}} + K_m^{BAM}} \quad (S8)$$

$$r_{deg}^{DCBA} = \mu_{max} \cdot \frac{\rho_{bio}}{Y} \cdot \frac{c_{bulk}^{DCBA}}{K_m^{DCBA} + c_{int}^{DCBA}} \cdot \frac{c_{bulk}^{O_2}}{K_m^{O_2} + c_{bulk}^{O_2}} \quad (S9)$$

$$r_{deg}^{O_2} = p \cdot r_{deg}^{DCBA} \quad (S10)$$

Parameter Uncertainties and Sensitivities

We fitted the log-parameter values (n = 10) using *lsqnonlin*, a MATLAB built-in nonlinear least squares data-fitting function, via minimization between model computed and measured concentration values. The delogarithmized fitted parameter values are presented alongside additional, fixed, physical parameters in

Table S2.

Results of a local sensitivity analysis, performed by perturbing each parameter value by 10% and comparing the model outcome to that of the optimal case, are presented for all relevant model output in Figure . The sensitivities presented in Figure are calculated by comparing the model outcome to measurements at each depth-location. Thus, Figure shows the spatial dependence of each parameter's sensitivity, that is, where along the depth profile does a parameter most influence the model outcome. A linearized uncertainty quantification was performed on the log-parameter values considering the sum of squared residuals (obtained from *lsqnonlin*) and parameter sensitivities obtained from the local sensitivity analysis. The relative parameter uncertainties are presented, for each parameter, along the legend of Figure . Thus, the relative uncertainty range for each parameter value is given by the multiple and quotient (\times / \div) of the fitted value and its relative uncertainty. That is, the closer the relative uncertainty is equal to 1, the more accurate the estimated parameter.

The results from our uncertainty quantification suggest that most parameters are well constrained, in particular, the parameters, k_{tr}^{BAM} , r_{max}^{hydro} , K_m^{BAM} , Y and X_{max} exhibited a narrow uncertainty range (low relative uncertainty) and these were also the parameters that the model outcome was most sensitive to. The relative uncertainty for k_{att} was not reported, because a 10% perturbation of the fitted parameter value did not yield a quantifiable change in the model output, and thus the absolute value of k_{att} was poorly constrained.

Table S2. Flow and transport parameters and reaction rate coefficients, for the reactive transport model, used as either fixed values obtained from the literature or fitted to measured data.

Symbol	Parameter	Values	Unit	References
Transport parameters				
d_{grain}	grain size	0.001	[m]	experimental
ϕ	porosity	0.45	[-]	experimental
α_l	longitudinal dispersivity	6×10^{-4}	[m]	fitted
α_t	transverse dispersivity	1.9×10^{-4}	[m]	$\alpha_t = d_{grain} \times 3 / 16$
D_m^{bio}	bacteria diffusion coefficient	1.5×10^{-11}	[m ² s ⁻¹]	Kathryn, et al. ¹³
D_m^{BAM}	diffusion coefficient	4.3×10^{-10}	[m ² s ⁻¹]	Jorgensen, et al. ¹⁴
$D_m^{O_2}$	diffusion coefficient	2.2×10^{-9}	[m ² s ⁻¹]	Ferrel and Himmelblau ¹⁵
Biokinetic parameters				
k_{tr}^{BAM}	mass transfer coefficient of BAM	7.6	[s ⁻¹]	fitted
k_{tr}^{DCBA}	mass transfer coefficient of DCBA	3.9	[s ⁻¹]	fitted
$k_{tr}^{O_2}$	mass transfer coefficient of O ₂	3×10^6	[s ⁻¹]	fitted
K_m^{BAM}	Michaelis Menten coefficient of BAM for the hydrolysis to form 2,6-DCBA	0.38	[$\mu\text{mol L}_{int}^{-1}$]	fitted
K_m^{DCBA}	Monod coefficient of 2,6-DCBA for further degradation	10.8	[$\mu\text{mol L}_{int}^{-1}$]	fitted
$K_m^{O_2}$	Monod coefficient of O ₂ for further degradation of DCBA	3.9	[$\mu\text{mol L}_{int}^{-1}$]	fitted
r_{max}^{hydro}	maximum hydrolysis rate constant from BAM to 2,6-DCBA	67.3	[$\mu\text{mol L}_{int}^{-1} \text{s}^{-1}$]	fitted
k_{att}	bacterial attachment rate constant	6.2×10^{-6}	[s ⁻¹]	fitted
μ_{max}	maximum specific growth rate constant	1.5×10^{-5}	[s ⁻¹]	fitted
X_{max}	maximum carrying capacity for biomass growth	97	[$\mu\text{mol}_{biomass} \text{L}^{-1}$]	fitted
Y	yield coefficient	0.24	[$\mu\text{mol}_{biomass} \mu\text{mol}^{-1}$]	fitted
V_{cell}	single cell volume	0.9	[μm^3]	Ellegaard, et al. ¹⁰
M_{cell}	dry weight per cell volume	3×10^{-7}	[$\mu\text{g}_{biomass}$]	Schultz-Jensen, et al. ⁴
ρ_{bio}	biomass density	3×10^6	[$\mu\text{mol}_{biomass} \text{L}_{int}^{-1}$]	$\rho_{bio} = M_{cell} / V_{cell}$
Isotope parameters				
ϵ^C	C isotope enrichment factor	-8	[‰]	Reinicke, et al. ¹⁶
ϵ^N	N isotope enrichment factor	-13.7	[‰]	Reinicke, et al. ¹⁶
Inflow concentrations				
c_{in}^{BAM}	BAM inlet concentration	100	[$\mu\text{mol L}^{-1}$]	experimental
$c_{in}^{O_2}$	O ₂ inlet concentration	244	[$\mu\text{mol L}^{-1}$]	experimental
X_{in}^{bio}	Biomass inlet concentration	32.6	[$\mu\text{mol L}^{-1}$]	fitted

The fitted parameters in the model were obtained via the automated model calibration. Other parameters were determined either by laboratory measurements or from literature.

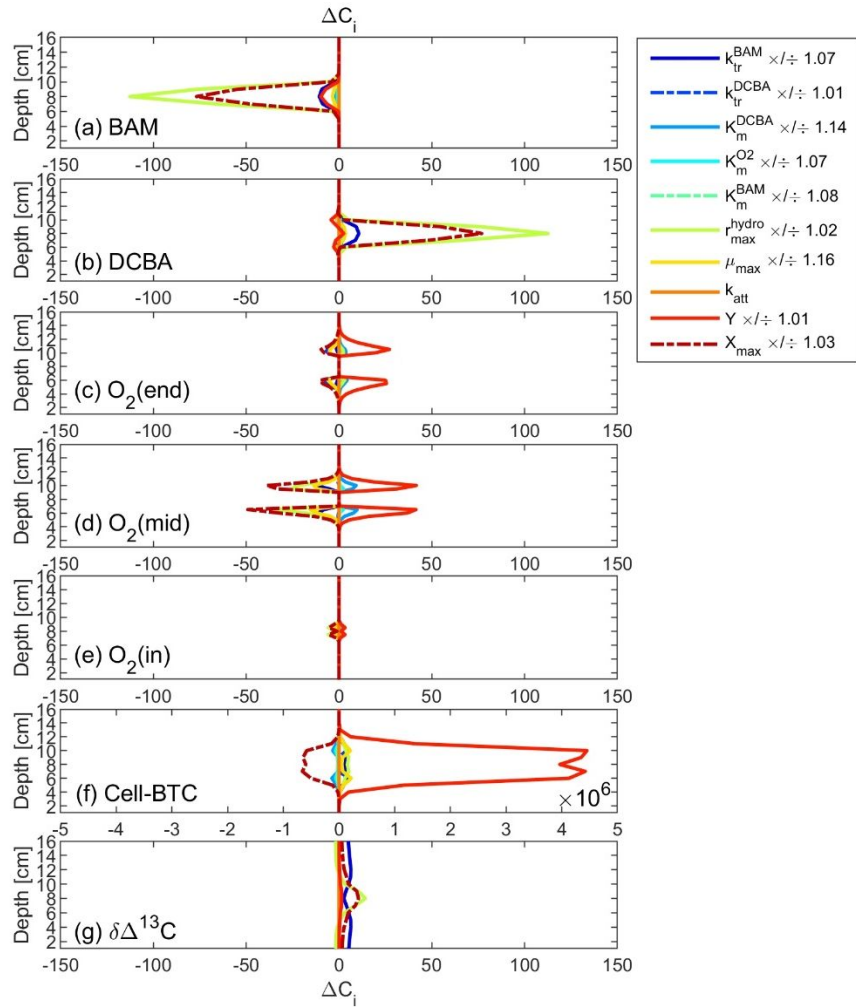


Figure S1. Parameter sensitivities plotted at each measurement location along the column depth-profile, where C_i denotes the i -th model outcome and p_j the j -th parameter ($n = 10$). Relative parameter errors (that is, \times / \div the fitted parameter value) are presented alongside each parameter in the figure legend. Parameters with a relative error close to 1 are well constrained. The uncertainty for k_{att} is not reported, because a 10% perturbation of the parameter did not yield a change in the model output.

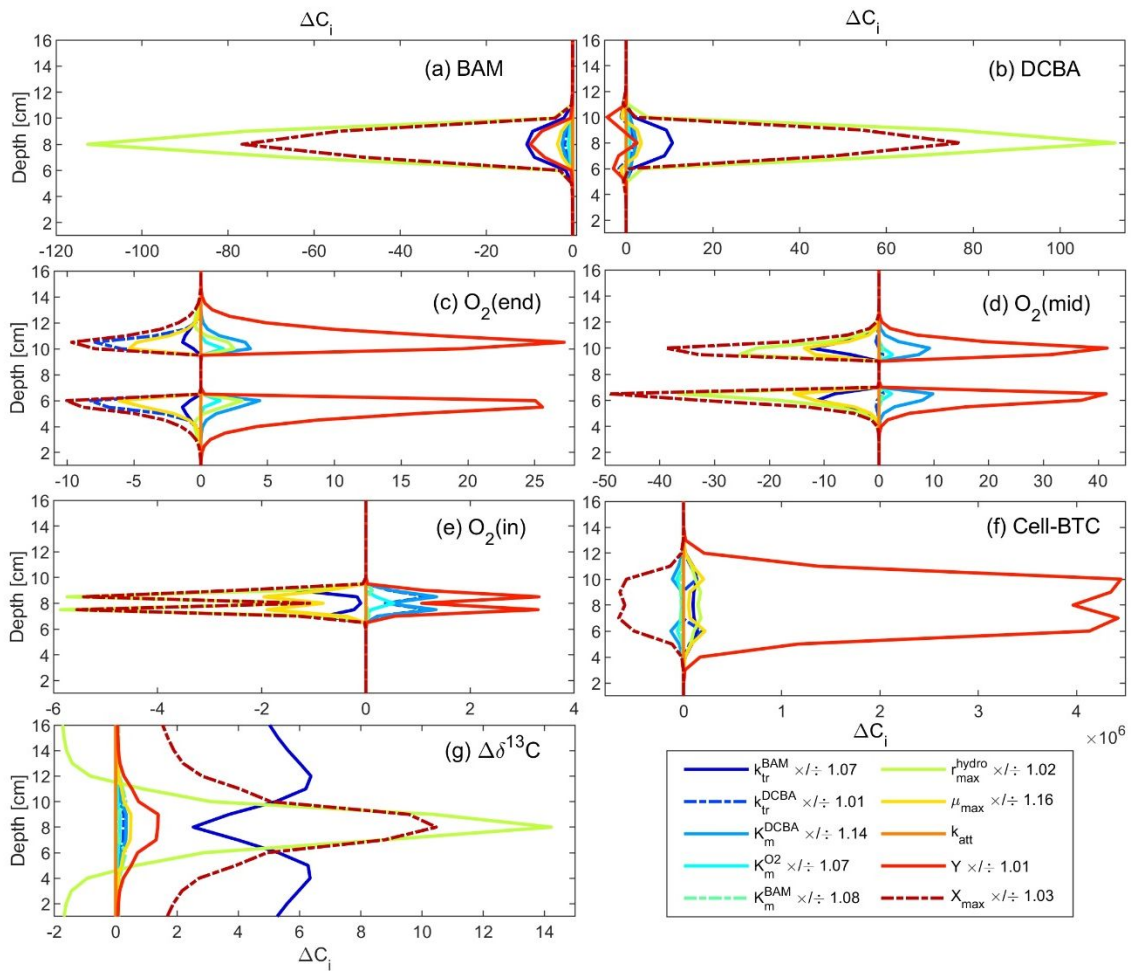


Figure S1 plotted in different x -scales.

Derivation of the Apparent Enrichment Factor (Equation 18)

The theoretical background of the derivation of eq 18 is based Thullner et al.¹⁷ Governing equations without consideration of isotopologues:

$$\frac{\partial c_{\text{bulk}}}{\partial t} = \frac{X^{\text{im}}}{\rho_{\text{bio}}} \cdot k_{\text{tr}} \cdot (c_{\text{int}} - c_{\text{bulk}}) \quad (\text{S11})$$

$$\frac{\partial c_{\text{int}}}{\partial t} = k_{\text{tr}} \cdot (c_{\text{bulk}} - c_{\text{int}}) - r_{\text{max}}^{\text{hydro}} \cdot \frac{c_{\text{int}}}{c_{\text{int}} + K_{\text{m}}} \quad (\text{S12})$$

Assume quasi-steady state in the bacterial cell interior:

$$k_{\text{tr}} \cdot (c_{\text{bulk}} - c_{\text{int}}) - r_{\text{max}}^{\text{hydro}} \cdot \frac{c_{\text{int}}}{c_{\text{int}} + K_{\text{m}}} = 0 \quad (\text{S13})$$

$$\Rightarrow (c_{\text{bulk}} - c_{\text{int}}) \cdot (c_{\text{int}} + K_{\text{m}}) - \frac{r_{\text{max}}^{\text{hydro}}}{k_{\text{tr}}} \cdot c_{\text{int}} = 0 \quad (\text{S14})$$

$$\Rightarrow -c_{\text{int}}^2 + \left(c_{\text{bulk}} - K_{\text{m}} - \frac{r_{\text{max}}^{\text{hydro}}}{k_{\text{tr}}} \right) \cdot c_{\text{int}} + c_{\text{bulk}} \cdot K_{\text{m}} = 0 \quad (\text{S15})$$

yields the quasi steady-state interior concentration:

$$\Rightarrow c_{\text{int}} = \frac{c_{\text{bulk}} - K_{\text{m}} - \frac{r_{\text{max}}^{\text{hydro}}}{k_{\text{tr}}} + \sqrt{\left(c_{\text{bulk}} - K_{\text{m}} - \frac{r_{\text{max}}^{\text{hydro}}}{k_{\text{tr}}} \right)^2 + 4c_{\text{bulk}} \cdot K_{\text{m}}}}{2} \quad (\text{S16})$$

Now we consider the light and heavy isotopologues:

$$\frac{\partial c_{\text{bulk}}^{\text{light}}}{\partial t} = \frac{X^{\text{im}}}{\rho_{\text{bio}}} \cdot k_{\text{tr}} \cdot (c_{\text{int}}^{\text{light}} - c_{\text{bulk}}^{\text{light}}) \quad (\text{S17})$$

$$\frac{\partial c_{\text{int}}^{\text{light}}}{\partial t} = k_{\text{tr}} \cdot (c_{\text{bulk}}^{\text{light}} - c_{\text{int}}^{\text{light}}) - r_{\text{max}}^{\text{hydro}} \cdot \frac{c_{\text{int}}^{\text{light}}}{c_{\text{int}}^{\text{light}} + K_{\text{m}}} \quad (\text{S18})$$

$$\frac{\partial c_{\text{bulk}}^{\text{heavy}}}{\partial t} = \frac{X^{\text{im}}}{\rho_{\text{bio}}} \cdot k_{\text{tr}} \cdot (c_{\text{int}}^{\text{heavy}} - c_{\text{bulk}}^{\text{heavy}}) \quad (\text{S19})$$

$$\frac{\partial c_{\text{int}}^{\text{heavy}}}{\partial t} = k_{\text{tr}} \cdot (c_{\text{bulk}}^{\text{heavy}} - c_{\text{int}}^{\text{heavy}}) - \alpha \cdot r_{\text{max}}^{\text{hydro}} \cdot \frac{c_{\text{int}}^{\text{heavy}}}{c_{\text{int}}^{\text{heavy}} + K_{\text{m}}} \quad (\text{S20})$$

With c_{int} as derived above, quasi-steady state in the interior implies:

$$k_{tr} \cdot (c_{bulk}^{light} - c_{int}^{light}) - r_{max}^{hydro} \cdot \frac{c_{int}^{light}}{c_{int} + K_m} = 0 \quad (S21)$$

$$k_{tr} \cdot (c_{bulk}^{heavy} - c_{int}^{heavy}) - \alpha \cdot r_{max}^{hydro} \cdot \frac{c_{int}^{heavy}}{c_{int} + K_m} = 0 \quad (S22)$$

$$\Rightarrow c_{int}^{light} = \frac{c_{bulk}^{light}}{1 + \frac{r_{max}^{hydro}}{k_{tr} \cdot (c_{int} + K_m)}} \quad (S23)$$

$$\Rightarrow c_{int}^{heavy} = \frac{c_{bulk}^{heavy}}{1 + \frac{\alpha \cdot r_{max}^{hydro}}{k_{tr} \cdot (c_{int} + K_m)}} \quad (S24)$$

Rate of change of concentration in the bulk phase:

$$\frac{\partial c_{bulk}^{light}}{\partial t} = \frac{X^{im}}{\rho_{bio}} \cdot k_{tr} \cdot (c_{int}^{light} - c_{bulk}^{light}) = \frac{X^{im}}{\rho_{bio}} \cdot k_{tr} \cdot c_{bulk}^{light} \cdot \left(\frac{1}{1 + \frac{r_{max}^{hydro}}{k_{tr}(c_{int} + K_m)}} - 1 \right) \quad (S25)$$

$$\frac{\partial c_{bulk}^{heavy}}{\partial t} = \frac{X^{im}}{\rho_{bio}} \cdot k_{tr} \cdot (c_{int}^{heavy} - c_{bulk}^{heavy}) = \frac{X^{im}}{\rho_{bio}} \cdot k_{tr} \cdot c_{bulk}^{heavy} \cdot \left(\frac{1}{1 + \frac{\alpha \cdot r_{max}^{hydro}}{k_{tr} \cdot (c_{int} + K_m)}} - 1 \right) \quad (S26)$$

Apparent fractionation factor:

$$\alpha^* = \frac{\frac{dc_{bulk}^{heavy}}{dt} \cdot c_{bulk}^{light}}{\frac{dc_{bulk}^{light}}{dt} \cdot c_{bulk}^{heavy}} \quad (S27)$$

$$= \frac{\frac{1}{1 + \frac{\alpha \cdot r_{max}^{hydro}}{k_{tr} \cdot (c_{int} + K_m)}} - 1}{\frac{1}{1 + \frac{r_{max}^{hydro}}{k_{tr} \cdot (c_{int} + K_m)}} - 1}$$

$$\begin{aligned}
& \frac{c_{\text{int}} + K_m}{\alpha \cdot r_{\text{max}}^{\text{hydro}} - 1} - 1 \\
& c_{\text{int}} + K_m + \frac{\alpha \cdot r_{\text{max}}^{\text{hydro}}}{k_{\text{tr}}} \\
= & \frac{c_{\text{int}} + K_m}{\frac{r_{\text{max}}^{\text{hydro}}}{k_{\text{tr}}} - 1} - 1 \\
& c_{\text{int}} + K_m + \frac{r_{\text{max}}^{\text{hydro}}}{k_{\text{tr}}} \\
& \alpha \\
& c_{\text{int}} + K_m + \frac{\alpha \cdot r_{\text{max}}^{\text{hydro}}}{k_{\text{tr}}} \\
= & \frac{\alpha}{1} \\
& c_{\text{int}} + K_m + \frac{r_{\text{max}}^{\text{hydro}}}{k_{\text{tr}}} \\
= & \alpha \frac{c_{\text{int}} + K_m + \frac{r_{\text{max}}^{\text{hydro}}}{k_{\text{tr}}}}{c_{\text{int}} + K_m + \frac{\alpha \cdot r_{\text{max}}^{\text{hydro}}}{k_{\text{tr}}}}
\end{aligned}$$

Substitute eq S16 into eq S27, we will get the final equation:

$$\alpha^* = \alpha \frac{c_{\text{bulk}} + K_m + \frac{r_{\text{max}}^{\text{hydro}}}{k_{\text{tr}}} + \sqrt{\left(c_{\text{bulk}} - K_m - \frac{r_{\text{max}}^{\text{hydro}}}{k_{\text{tr}}}\right)^2 + 4c_{\text{bulk}} \cdot K_m}}{c_{\text{bulk}} + K_m + (2\alpha - 1) \cdot \frac{r_{\text{max}}^{\text{hydro}}}{k_{\text{tr}}} + \sqrt{\left(c_{\text{bulk}} - K_m - \frac{r_{\text{max}}^{\text{hydro}}}{k_{\text{tr}}}\right)^2 + 4c_{\text{bulk}} \cdot K_m}} \quad (\text{S28})$$

The calculation based on eq 18 and the one based on Thullner et al (eq S29) yielded same estimations (Figure 4).

$$\alpha^* = \alpha \cdot \frac{1 + \frac{1}{2} \left(\frac{a}{k_{\text{tr}}} - \frac{c_{\text{bulk}}}{K_m} - 1 \right) + \sqrt{\frac{a}{k_{\text{tr}}} + \frac{1}{4} \cdot \left(\frac{a}{k_{\text{tr}}} - \frac{c_{\text{bulk}}}{K_m} - 1 \right)^2}}{1 + \alpha_0 \cdot \left[\frac{1}{2} \left(\frac{a}{k_{\text{tr}}} - \frac{c_{\text{bulk}}}{K_m} - 1 \right) + \sqrt{\frac{a}{k_{\text{tr}}} + \frac{1}{4} \cdot \left(\frac{a}{k_{\text{tr}}} - \frac{c_{\text{bulk}}}{K_m} - 1 \right)^2} \right]} \quad (\text{S29})$$

Additional Supporting Figures

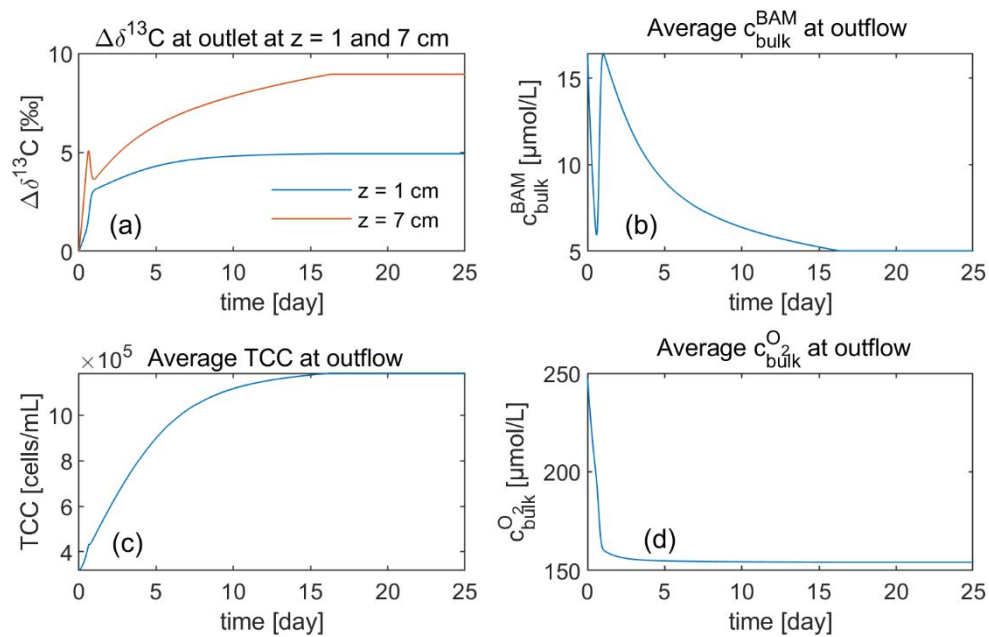


Figure S2. Simulated transient development of isotope values $\Delta\delta^{13}\text{C}$, BAM concentration $c_{\text{bulk}}^{\text{BAM}}$, total washed-out cell number TCC , and oxygen concentration $c_{\text{bulk}}^{\text{O}_2}$ at outflow. System reached to steady state on day 17.

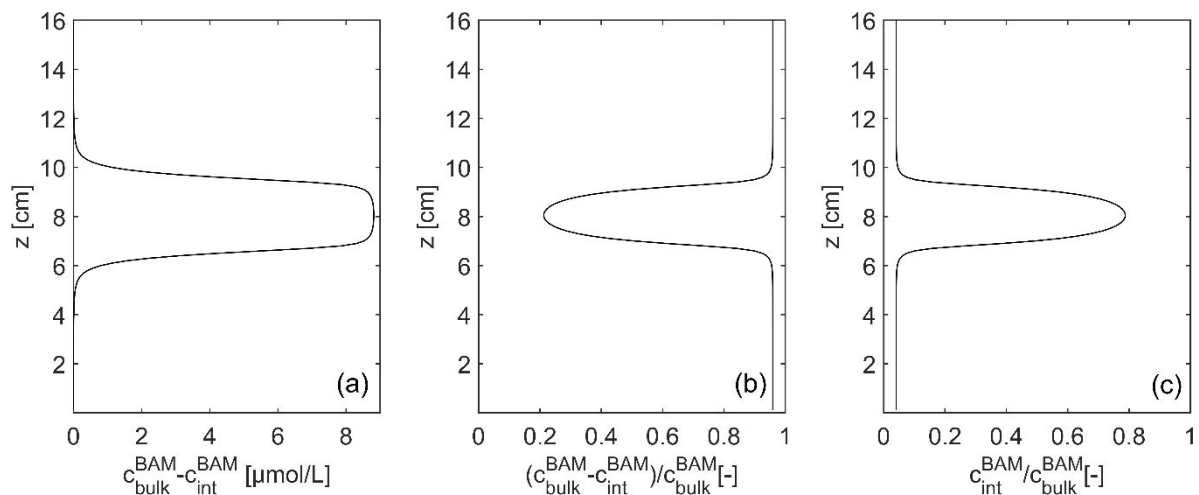


Figure S3. Concentration difference between the bulk solution $c_{\text{bulk}}^{\text{BAM}}$ and the intracellular solution $c_{\text{int}}^{\text{BAM}}$ along the vertical outlet profile.

References

1. Torrentó, C.; Bakkour, R.; Ryabenko, E.; Ponsin, V.; Prasuhn, V.; Hofstetter, T. B.; Elsner, M.; Hunkeler, D. Fate of four herbicides in an irrigated field cropped with corn: lysimeter experiments. *Procedia Earth Planet. Sci.* **2015**, *13*, 158-161.
2. Jensen, G. G.; Bjorklund, E.; Simonsen, A.; Halling-Sorensen, B. Determination of 2,6-dichlorobenzamide and its degradation products in water samples using solid-phase extraction followed by liquid chromatography-tandem mass spectrometry. *J. Chromatogr. A* **2009**, *1216* (27), 5199-206.
3. Sun, F.; Peters, J.; Thullner, M.; Cirpka, O. A.; Elsner, M. Magnitude of diffusion- and transverse dispersion-induced isotope fractionation of organic compounds in aqueous systems. *Environ. Sci. Technol.* **2020**, *submitted for publication*.
4. Schultz-Jensen, N.; Knudsen, B. E.; Frkova, Z.; Aamand, J.; Johansen, T.; Thykaer, J.; Sorensen, S. R. Large-scale bioreactor production of the herbicide-degrading *Aminobacter* sp. strain MSH1. *Appl. Microbiol. Biotechnol.* **2014**, *98* (5), 2335-44.
5. Shinoda, W. Permeability across lipid membranes. *Biochim. Biophys. Acta, Biomembr.* **2016**, *1858* (10), 2254-2265.
6. Males, R.; Herring, F. A ¹H-NMR study of the permeation of glycolic acid through phospholipid membranes. *Biochim. Biophys. Acta, Biomembr.* **1999**, *1416* (1-2), 333-338.
7. Ehrl, B. N.; Kundu, K.; Gharasoo, M.; Marozava, S.; Elsner, M. Rate-limiting mass transfer in micropollutant degradation revealed by isotope fractionation in chemostat. *Environ. Sci. Technol.* **2019**, *53* (3), 1197-1205.
8. Ulrich, N.; Endo, S.; Brown, T. N.; Watanabe, N.; Bronner, G.; Abraham, M. H.; Goss, K. U. UFZ-LSER database v 3.2 [Internet]. **2017**.
9. Young, K. D. The selective value of bacterial shape. *Microbiol. Mol. Biol. Rev.* **2006**, *70* (3), 660-703.
10. Ellegaard-Jensen, L.; Albers, C. N.; Aamand, J. Protozoa graze on the 2, 6-dichlorobenzamide (BAM)-degrading bacterium *Aminobacter* sp. MSH1 introduced into waterworks sand filters. *Appl. Microbiol. Biotechnol.* **2016**, *100* (20), 8965-8973.
11. Ehrl, B. N.; Gharasoo, M.; Elsner, M. Isotope Fractionation Pinpoints Membrane Permeability as a Barrier to Atrazine Biodegradation in Gram-negative *Polaromonas* sp. Nea-C. *Environ. Sci. Technol.* **2018**, *52* (7), 4137-4144.
12. Ayman, E.-H.; Jayaram, S. H. In *Effect of biological cell size and shape on killing efficiency of pulsed electric field*, 2008 IEEE International Conference on Dielectric Liquids, IEEE: 2008; pp 1-4.
13. Strobel, K. L.; McGowan, S.; Bauer, R. D.; Griebler, C.; Liu, J.; Ford, R. M. Chemotaxis increases vertical migration and apparent transverse dispersion of bacteria in a bench - scale microcosm. *Biotechnol. Bioeng.* **2011**, *108* (9), 2070-2077.
14. Jorgensen, P. R.; Klint, K. E.; Kistrup, J. P. Monitoring well interception with fractures in clayey till. *Ground Water* **2003**, *41* (6), 772-9.
15. Ferrell, R. T.; Himmelblau, D. M. Diffusion coefficients of nitrogen and oxygen in water. *J. Chem. Eng. Data* **1967**, *12* (1), 111-115.
16. Reinnicke, S.; Simonsen, A.; Sorensen, S. R.; Aamand, J.; Elsner, M. C and N isotope fractionation during biodegradation of the pesticide metabolite 2,6-dichlorobenzamide (BAM): potential for environmental assessments. *Environ. Sci. Technol.* **2012**, *46* (3), 1447-54.
17. Thullner, M.; Kampara, M.; Richnow, H. H.; Harms, H.; Wick, L. Y. Impact of bioavailability restrictions on microbially induced stable isotope fractionation. 1. Theoretical calculation. *Environ. Sci. Technol.* **2008**, *42* (17), 6544-6551.